Formosa Journal of Science and Technology (FJST)
Vol.3, No.5, 2024: 899-916

# CFD Simulation of Biomass Pyrolysis in a Fluidized Bed Reactor: Effect of Particle Shrinkage Model

Thoharudin
Department of Mechanical Engineering, Universitas Muhammadiyah Yogyakarta (UMY), Yogyakarta
**Corresponding Author:** Thoharudin, thoharudin@ft.umy.ac.id

A R T I C L E I N F O

*Keywords:* Biomass, Pyrolysis, Multistep Comprehensive Reaction, Fluidized Bed Reactor, Particle Shrinkage

*Received : 12, March*
*Revised : 15, April*
*Accepted: 20, May*



A B S T R A C T

This study implemented the improved multistep comprehensive reaction for pyrolysis in a fluidized bed reactor. Particle shrinkage models were developed with variations of constant and nonconstant particle size with different char densities. Different biomass particle sizes were also investigated to observe their decomposition characteristic in a fluidized bed reactor. A multifluid model framework integrated with heterogeneous chemical reactions was developed to simulate fast biomass pyrolysis in a 2-D computational domain. The improved multistep comprehensive reaction exhibited good agreement with experimental pyrolysis product yields and their compositions. Shrinkage models with constant particle size promoted segregation and tended to generate coarse gradients between the dense zone and the freeboard. By contrast, the shrinkage models with nonconstant particle size favored more homogeneous biomass and char & metaplastic mass fractions in the reactor and reduced segregation. Models 4–6 exhibited positive representations of particle shrinkage with particle volume reductions of 54.4%, 54.3% and 50.7%, respectively.

DOI Prefix: https://doi.org/10.55927/fjst.v3i5.9435
ISSN-E: 2964-6804
https://journal.formosapublisher.org/index.php/fjst

## INTRODUCTION

Biomass fast pyrolysis is a promising solid fuel conversion technology due to its rapid process and high conversion efficiency [1]. Fast pyrolysis implements a rapid heating rate in a moderate temperature (~500 °C) with a short residence time to maximize the liquid product in an environment where oxygen is absent [2]. Pyrolysis is preferred over other types of thermochemical conversion due to the liquid form (bio-oil) of the main product; in which, the upgraded bio-oil is a highly dense and useful form of energy with simple storage and transportation requirements [3]. A fluidized bed reactor is a common pyrolysis reactor that offers benefits including continuous operation, simple design, uniform reactor temperature, excellent heat and mass transfers, and solid mixing [4].

Numerous simulations have recently been conducted to investigate pyrolysis in fluidized bed reactors, including the study [5] that explored the yields of palm kernel shell pyrolysis. Jalalifar et al. [6] investigated the parameters influencing pyrolysis yields. Clissold et al. [4] elucidated the interphase heat transfer and fluidization behavior of pyrolysis in a fluidized bed reactor. Their pyrolysis reaction used the simple reaction (global reaction mechanism) proposed by Miller and Bellan [7], which has a limitation of information on the quality of the pyrolysis products. The multistep comprehensive mechanism, first proposed by Ranzi et al. [8], employs obvious species, which enables exploring both pyrolysis product quantity (pyrolysis yields) and quality, including the gas compositions, bio-oil, and solid residue species, with their elemental compositions. The comprehensive multistep mechanism has undergone many improvements. Anca-Couce et al. [9] modified the reaction by considering the secondary charring reaction (validated using the Thermogravimetric analysis (TGA) method). Gentile et al. [10] implemented extractive component thermal degradation (validated using biomass pellet evolution, including the mass fraction and visual character). Debiagi et al. [11] improved the accuracy of the mechanism to predict the solid residue yield and its elemental compositions (validated in numerous experiments). Debiagi et al. [11] also divided the hemicellulose into three distinct compositions, namely softwood hemicellulose, hardwood hemicellulose, and grass hemicellulose.

Nonetheless, applications of the multistep comprehensive mechanism in fluidized bed pyrolysis remain limited. Mellin et al. [12] and Ranganathan et al. [13] reported pyrolysis in a fluidized bed reactor by using a multistep comprehensive reaction that neglected metaplastic decompositions. The recent work reported by Lu et al. [14] investigating fluidized bed pyrolysis used the multistep comprehensive mechanism modified by Debiagi et al. [11]. Lu et al. [14] focused on the pyrolysis product yields of a variety of biomass and the impact of particle size. The pyrolysis product yields reflected those in the experiments; the compositions of bio-oil and solid residue exhibited observable differences. For example, the amount of carbon elements of bio-oil and solid residue were lower than in the experiments, while their oxygen elements were higher.

In fluidized bed pyrolysis, the biomass is rapidly degraded through the release of volatile matter and solid residue particles remain. Both should be quickly removed from the reactor to avoid the secondary cracking of tar and the catalytic effect of char reducing tar/bio-oil yields; however, too fast particle removal promote the increase of unreacted biomass (UB) in the solid residue [15]. During the devolatilization process, the biomass particles shrink in density and diameter, affecting hydrodynamics behavior, heat transfer, and reaction rate [16–18]. Hence, in a fluidized bed pyrolysis simulation, particle shrinkage should be modeled to observe a more realistic solid particle flow in the reactor. However, most studies have neglected the particle shrinkage effect and considered the biomass particle as having a constant size during devolatilization. Zhong et al. [16] developed biomass particle shrinkage models based on the density and mass fraction of solid species calculation by considering the mass conservation at a particle scale, which was a convenient method with low computational requirements. They used numerous simple pyrolysis mechanisms to illustrate the biomass pyrolysis in a fluidized bed reactor, resulting in a disparity between hydrodynamics behavior and pyrolysis product yields; however, their particle shrinkage models were limited by dependency on the specific pyrolysis mechanism and temperature [16,18]. To the authors' knowledge, no study has correlated particle shrinkage to the multistep comprehensive mechanism to elucidate the particle shrinkage effect on pyrolysis product distributions. Moreover, many char density models used in pyrolysis simulations are not investigated comprehensively for hydrodynamics behavior and pyrolysis product distributions.

This study compared the most recent modified multistep comprehensive pyrolysis mechanism (Anca-Couce et al. [9], Gentile et al. [10], and Debiagi et al. [11]) in a fluidized bed reactor and proposed a modification to improve the accuracy in predicting the gas, bio-oil, and solid residue yields and compositions applicable in the fluidized bed condition (dense and dilute multiphase flows). Particle shrinkage was modeled based on the shrinking unreacted particle model (SUPM), which offered more flexibility in the use and was widely used for biomass particle shrinkage model in the gasification simulations [19]. The different char densities were also investigated associated with studies reporting disparities in char density, including the char density lower than that of biomass [20], identical to that of biomass [21], and higher than that of biomass [4,5] to elucidate the particle behavior and biomass conversion characteristic in a fluidized bed reactor.

## THEORETICAL FRAMEWORK

The comprehensive multistep mechanism has undergone many improvements. Anca-Couce et al. [9] modified the reaction by considering the secondary charring reaction (validated using the Thermogravimetric analysis (TGA) method). Gentile et al. [10] implemented extractive component thermal degradation (validated using biomass pellet evolution, including the mass fraction and visual character). Debiagi et al. [11] improved the accuracy of the mechanism to predict the solid residue yield and its elemental compositions (validated in numerous experiments). Debiagi et al. [11] also divided the

hemicellulose into three distinct compositions, namely softwood hemicellulose, hardwood hemicellulose, and grass hemicellulose.

Nonetheless, applications of the multistep comprehensive mechanism in fluidized bed pyrolysis remain limited. Mellin et al. [12] and Ranganathan et al. [13] reported pyrolysis in a fluidized bed reactor by using a multistep comprehensive reaction that neglected metaplastic decompositions. The recent work reported by Lu et al. [14] investigating fluidized bed pyrolysis used the multistep comprehensive mechanism modified by Debiagi et al. [11]. Lu et al. [14] focused on the pyrolysis product yields of a variety of biomass and the impact of particle size. The pyrolysis product yields reflected those in the experiments; the compositions of bio-oil and solid residue exhibited observable differences. For example, the amount of carbon elements of bio-oil and solid residue were lower than in the experiments, while their oxygen elements were higher.

## METHODOLOGY

The Eulerian–Eulerian framework, the so-called multifluid model (MFM) or two-fluid model, was chosen to account for continuity, momentum, and energy according to the Navier–Stokes equation integrated with heterogeneous chemical reactions because this approach requires less computational effort to solve multiphase flows with thousands or millions of particles. In general, the MFM treats particles as well as fluids as interpenetrating continua, and their interactions, including drag force, heat and mass transfer, and chemical reactions, are calculated using interphase exchange terms. The gas phase is considered the primary phase, and the solid phases are treated as secondary phases wherein the fluidized bed pyrolysis involves two solid phases (biomass and sand). The gas–particle drag force was modeled using the Gidaspow [22] equation; gas–particle heat transfer including gas–biomass and gas–sand were calculated based on the Gunn formula [23]; biomass and sand heat transfer was approached using Tomiyama's equation [24], which was used in the fluidized bed steam gasification model of Eri et al. [25]. The discrete ordinate (DO) model available in Ansys Fluent [26] software was used to simulate the radiation model, with a gas absorption coefficient of 0.07 $m^{-1}$ as previously implemented by Qian et al. [27].

To achieve increased effectiveness and short computation time, a 2-D domain was performed to model the fast pyrolysis in a fluidized bed reactor. The reactor geometry is illustrated in Fig. 1, where the diameter and height are 7.2 cm and 65 cm, respectively, according to the experimental work by Kantarelis et al. [28]. Biomass with a particle size of 0.85 mm consisting of pinewood and spruce mixture was fed into the reactor at 1 kg/h at 27 °C. The biomass mixture, comprising cellulose, hemicellulose, Lign-C, Lign-H, and Lign-O (46.7%, 30.2%, 2.55%, 8.0%, and 12.55%, respectively), was calculated using the average composition of pinewood and spruce as it also implemented in our earlier study [29]. Silica sand 300 μm in diameter was initially packed with a volume fraction of 0.55 and a height of 10 cm. Nitrogen as the fluidizing gas was injected at the pyrolysis temperature (500 °C) from the bottom of the

reactor at a superficial velocity of 0.25 m/s. The pyrolysis products including yields and their compositions were compared to the literature [12,28].

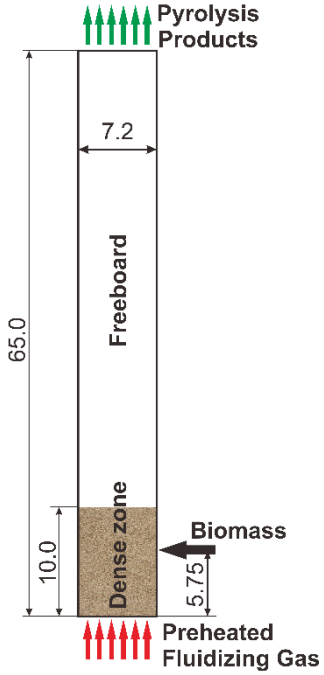


**Fig. 1. Illustration of 2-D fluidized bed reactor (unit, cm).**

The improved comprehensive mechanism was proposed in our earlier study [29–31]. This model was developed based on reported mechanisms (Anca-Couce et al. [9], Gentile et al. [10], and Debiagi et al. [11]), with different bio-oil species, enhanced carbon element in the solid residue, modified metaplastic decompositions, and simplification of the reaction steps. All reactions were expressed using the first-order Arrhenius equation, as given by

$$k_i = A_i \cdot \exp\left[-E_i / RT\right] \quad (1)$$

where $k_i$ denotes the kinetic constant of reaction rate, $A_i$ is the Arrhenius pre-exponential constant, and $E_i$ indicates the activation energy of the chemical reaction. $R$ and $T$ are the universal ideal gas constant and temperature, respectively. The reaction constants ($k_i$) and heats of reaction ($\Delta H$) were integrated using user-defined functions (UDFs) written in C++ code via DEFINE_HET_RXN_RATE and DEFINE_SOURCE macros, respectively.

During devolatilization, biomass particles reduce in density and size by releasing volatile matter and leaving solid residue, known as the shrinkage effect. In this work, the shrinkage effect was modeled using numerous variations, which are illustrated in Fig. 2. The apparent density of particles is influenced by the densities of biomass, char & metaplastic, and void; void density was treated as gas density according to the simulation by Liu et al. [21]. The apparent density of biomixture particle ($\rho_{ap}$) was calculated using volume weighted mixing law, as given by

$$\rho_{ap} = \frac{1}{\frac{Y_b}{\rho_b} + \frac{Y_c}{\rho_c} + \frac{Y_a}{\rho_a} + \frac{Y_v}{\rho_v}} \quad (2)$$

where $\rho$ and $Y$ denote density and mass fraction, respectively, and subscript $b$, $c$, $a$, and $v$ indicate the biomass, char & metaplastic, ash, and void, respectively.

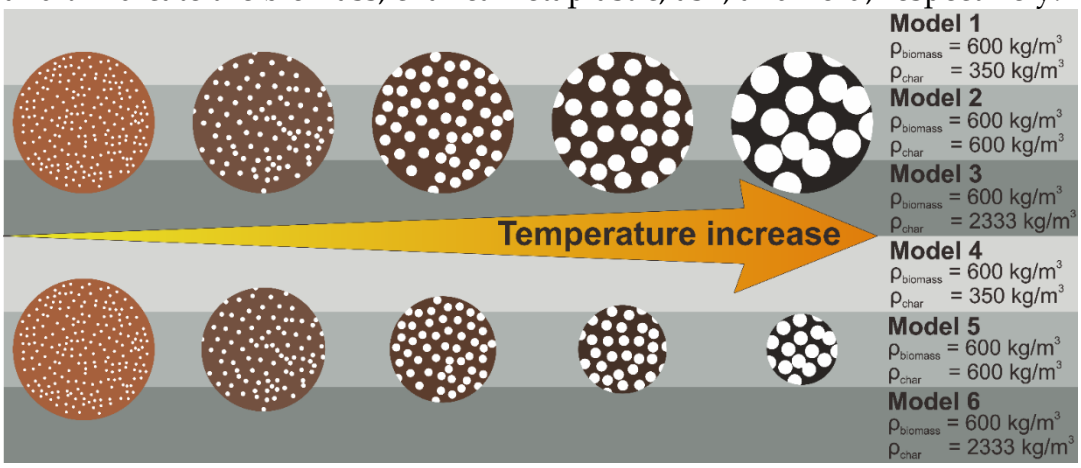


**Fig. 2. Particle shrinkage model illustration.**

As shown in Fig. 2, Models 1–3 represent the biomass particle shrinkage in density with a constant diameter where the simulations in section 3.1 were conducted using Model 1. Models 4–6 illustrate the biomass particle shrinkage in both density and diameter where the biomass particle shape was assumed to have a sphere geometry, with the particle size evolution calculated as follows [19,32]:

$$d_i = d_0(1 - X_c)^{1/3} \quad (3)$$

where $d_i$ and $d_0$ are the final and initial biomass diameter, respectively, while $X_c$ is the local carbon conversion which was adapted as the local biomass conversion for this pyrolysis case and was expressed by the char mass fraction. The relationship between the biomass particle size and char mass fraction is illustrated in Fig 3. The biomass particle size evolution equation was integrated using UDF through DEFINE_PROPERTY macros.

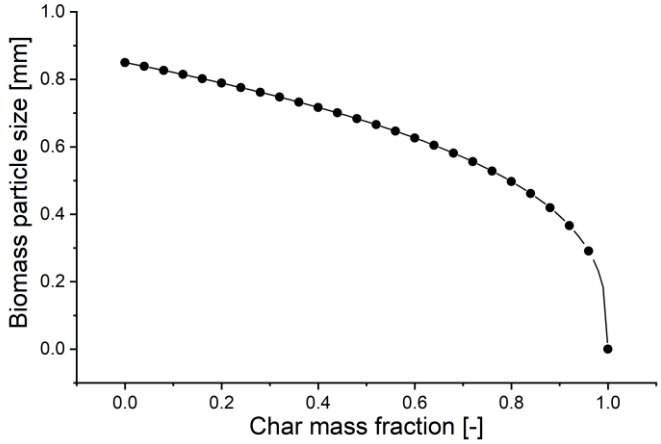


**Fig. 3. The relationship between char mass fraction and biomass particle size.**

## RESULT AND DISCUSSION

### *Pyrolysis Products Comparison*

Fig. 4a depicts the biomass mass fractions at the times the simulations exhibited the decrements of the biomass mass fractions. After 30 s, the decrements were negligible; thus, 40 s of simulation time was used in further work. Pyrolysis product yields for solid residue, noncondensable gas (NCG), and bio-oil (consisting of a mixture of organics and water) modeled using a kinetic mechanism of Anca-Couce et al. [9], Gentile et al. [10], Debiagi et al. [11], and this improved model is presented in Fig. 3b. The mechanism proposed by Anca-Couce et al. [9] included a secondary charring reaction that enhanced carbon, water, carbon dioxide, and hydrogen in the reaction steps, modified using the pyrolysis mechanism improved by Corbetta et al. [33].

Moreover, the formations of sugars such as levoglucosan and xylose monomer were substituted by those of other products because sugars are sensitive to temperature and mineral earth content in the biomass, affecting the organic yield decrement. As a result, the mechanism developed by Anca-Couce et al. [9] resulted in lower organics with higher NCG yields compared with those of Gentile et al. [10] and Debiagi et al. [11]. Gentile et al. [10] proposed a comprehensive pyrolysis mechanism with a high fraction of metaplastic phase and slow metaplastic decompositions; thus, this mechanism yielded a large fraction of solid residue with a small amount of NCG because much NCG was still trapped in the solid residue, as a metaplastic phase. Debiagi et al. [11] developed a comprehensive pyrolysis mechanism with a lower metaplastic phase; therefore, despite its slow metaplastic decomposition, it had a lower solid residue yield compared with the mechanism developed by Anca-Couce et al. [9] and Gentile et al. [10]. Both Gentile et al. [10] and Debiagi et al. [11] neglected the effect of secondary charring and the presence of mineral earth in the biomass; thus, a large percentage of the bio-oil was organic—larger than in the experiment. Nonetheless, the solid residue yield of the mechanism of Debiagi et al. [11] was close to that of the experiment, namely 17.73%.

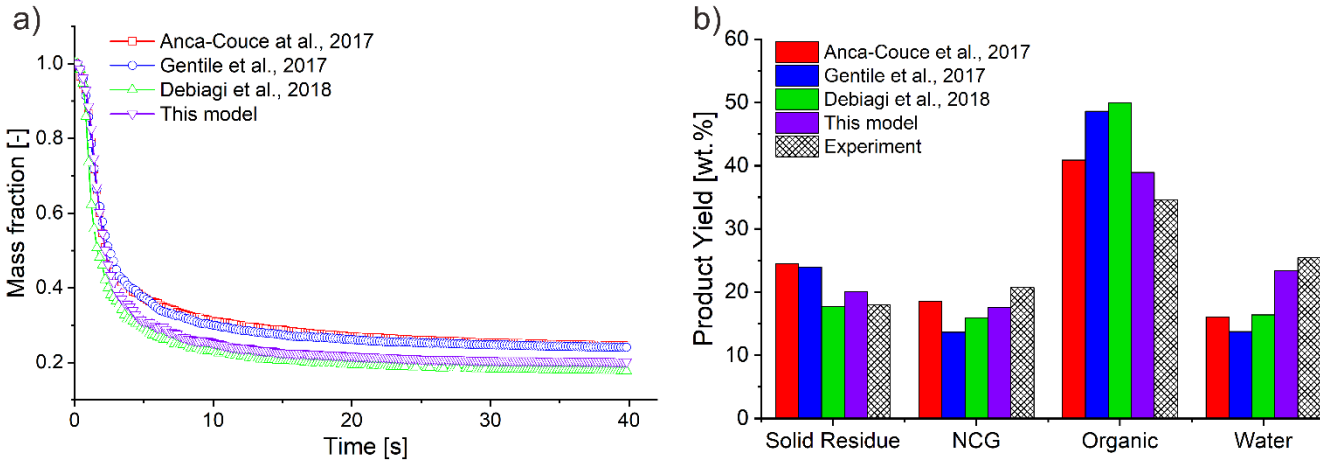


**Fig. 4. a) Simulated biomass mass fractions; b) pyrolysis product yields.**

After adopting the Debiagi et al. [11] mechanism with its low metaplastic fractions, considering the secondary charring reaction in which carbon and water product are enhanced, the existence of mineral earth in the biomass

(which removes the sugar compositions), and the bio-oil end-product species largely found in the experiment, the improved mechanism was constructed. The solid residue yield was somewhat higher than that of the experiment, but those of the other products, such as NCG, organics, and water, were comparable. Compared with the experiment, the improved model had relative errors of 11.8%, −15.2%, 12.6%, and −8.0% in predicting solid residue, NCG, organics, and water, respectively.

Pyrolysis is a complex thermochemical conversion where physical and chemical parameters contribute to the final products. The condenser temperature and gas feeding rate of the condenser were neglected in the simulation. In the study reported by Westerhof et al. [34], a higher condenser temperature of 30 °C reduced the amount of organics trapped in the condenser by approximately 2%–7%, depending on the gas feeding rate. The lignocellulosic interactions such as cellulose–hemicellulose and cellulose–lignin contributing to water, CO, and $CO_2$ formation and tar reduction were also neglected in the simulation. The secondary reactions converting organics into water vapor and NCG were also neglected in the simulation due to their little contribution, as the operating temperature was lower than 600 °C[33,35]. In short, the lower predicted NCG and water with higher organic components yields in the simulation using the improved model was reasonable due to the complexity of actual pyrolysis.

Bio-oil is a complex mixture of several hundred organic species; however, to simplify the model compound, only large species involved in multistep comprehensive mechanisms were included. The species can be categorized into groups such as sugars, aldehydes, ketones, carboxylic acids, and phenols. Pyrolysis of pinewood and spruce, softwood materials with high cellulose components, resulted in considerable production of ketones & aldehydes, carboxylic acids, and phenolics, with small amounts of furans and sugars, in the experiment (Fig. 5). Anca-Couce et al. [9] modeled hydroxyacetaldehyde (HAA) and formaldehyde as the main products of cellulose and hemicellulose pyrolysis; thus, the ketones & aldehydes components were much larger (by more than twice) than those obtained in the experiment. Carboxylic acids and phenolics percentages, mainly derived from hemicellulose and lignin (Lign-C, Lign-H, and Lign-O) pyrolysis, were lower than those in the experiment. In addition to sinapaldehyde and phenol as phenolics species in the Anca-Couce et al. [9] mechanism, formaldehyde and acetone were nonaromatic species derived from lignin pyrolysis; thus, the phenolics group was present in little amounts in bio-oil. Anca-Couce et al. [9] considered omitting levoglucosan formation as a sugar product due to the sensitivity of the product to mineral earth content in biomass, and this was relevant for the experiment (less than 2%; Fig. 6).

Similarly to Anca-Couce et al. [9], Gentile et al. [10] modeled organic species from cellulose and hemicellulose pyrolysis as consisting mainly of HAA and formaldehyde as the aldehydes product; however, considering levoglucosan as the product of cellulose degradation, levoglucosan was the most prevalent organic species in bio-oil. Carboxylic acids and phenolics

groups were also present in minute fractions, while the furans group exhibited a marginally higher fraction compared with the experiment. In short, the organic species modeled by Gentile et al. [10] consisted mainly of sugars and aldehydes.

Debiagi et al. [11] modeled organic species to predominantly comprise levoglucosan, similar to the Gentile et al. [10] model, with a slower levoglucosan formation reaction rate. The furans group existed as a large fraction almost equal to that of ketones & aldehydes. Carboxylic acids consisting of acetic acid and propionic acid had ~70% lower than that in the experiment because hemicellulose decomposition promoted furans and aldehydes in addition to carboxylic acids. Similarly to Anca-Couce et al. [9] and Gentile et al. [10], Debiagi et al. [11] modeled organic species derived from lignin comprising mainly aldehydes & ketones, with phenolics species present in a low fraction.

The improved model adopted Anca-Couce et al. [9] and removed levoglucosan as the product from cellulose pyrolysis and substituted it with its fragmentation products, including ketones & aldehydes and furans; thus, no sugars were present in the bio-oil product. Ketones & aldehydes existed in a proportion somewhat higher than that in the experiment. Carboxylic acids comprised mainly acetic acid and propionic acid obtained through hemicellulose pyrolysis exhibited a close relationship to the experimental results. The proportion of phenolics group including simple phenol and methoxy phenol was also highly correlated with that in the experiment. This model implemented phenolics derived from both lignin pyrolysis and from hemicellulose according experimental studies conducted by Michailof et al. [36] and Zhao et al. [37]. This improved model predicted carboxylic acids, ketones & aldehydes, furans, and phenolics of 11.5%, 20.9%, 17.5%, and 10.8%, respectively.

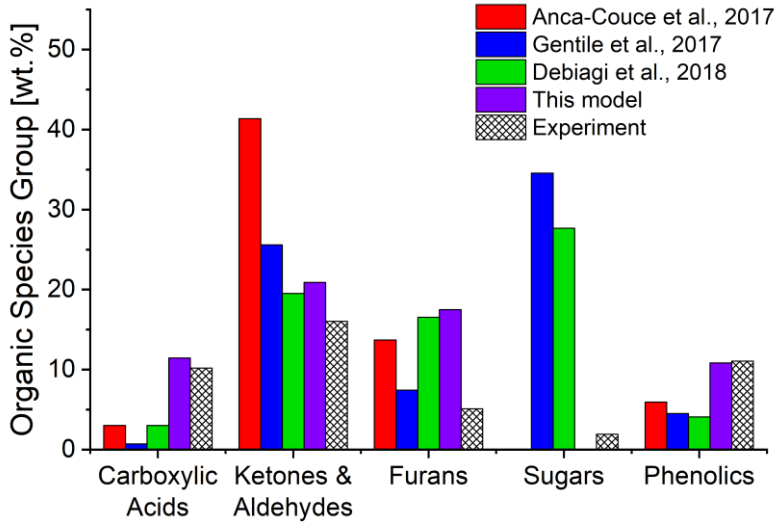


**Fig. 5. Organic species compositions.**

The C, H, and O compositions of bio-oil are presented in Fig. 6. Anca-Couce et al. [9], Gentile et al. [10], and Debiagi et al. [11] modeled bio-oil species predominantly consisting of sugars and ketones & aldehydes, and which had a low carbon content (<60 wt.%); thus, the bio-oil had less carbon content with

higher oxygen composition compared with the experiment values. Differently from the other mechanisms, the improved model implemented high carbon content bio-oil species (C ≥ 60 wt.%) in large fractions, such as acetone, furfural, hydroxymethylfurfural (HMFU), and phenol; therefore, the elemental compositions had high carbon content quite close to that in the experiment, namely C, H, and O of 56.3%, 6.9%, and 36.8% with the relative errors of −2.3%, 3.6%, and 3.0%, respectively.

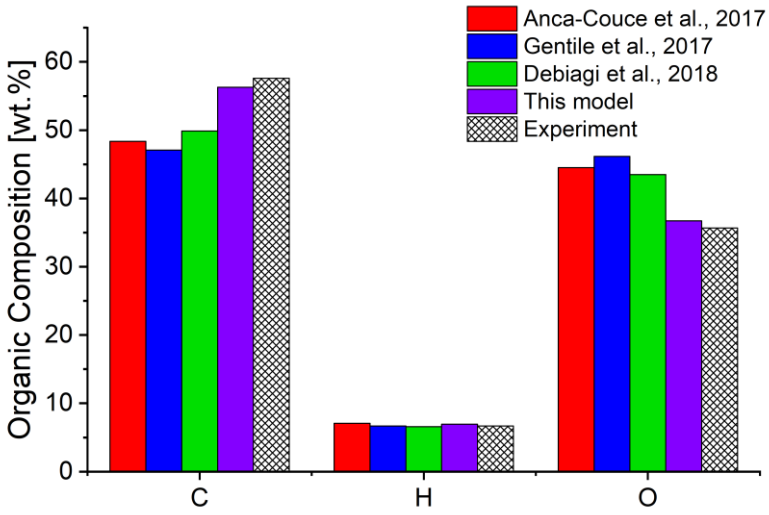


**Fig. 6. Organic elemental composition.**

***Particle Shrinkage Model***

Fig. 7 presents the biomass temperature distributions of the particle shrinkage models. In general, they exhibited nonsignificant differences in biomass temperature distribution, where the temperature of the biomass suddenly increased from 27 °C to 500 °C, similarly to the phenomenon described by Lu et al. [14]. As a consequence, the biomass mass fraction quickly decreased by approximately half in the dense zone and gradually decreased in the freeboard, as illustrated in Fig. 8a. By contrast, the char & metaplastic mass fraction quickly increased by approximately 50% in the dense zone and gradually increased in the freeboard (Fig. 8b). The distinct phenomenon appeared on the gradient between the dense zone and the freeboard wherein a coarse gradient was exhibited in the constant particle size models, and it became coarser with increasing char density. By contrast, after particle size shrinkage was implemented, the gradient between the dense zone and the freeboard emerged smoothly, particularly observed in Model 4.

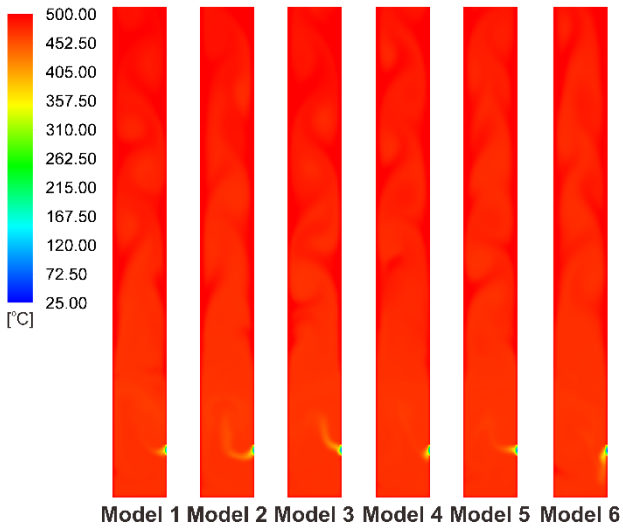


Fig. 7. Biomass temperature distribution.

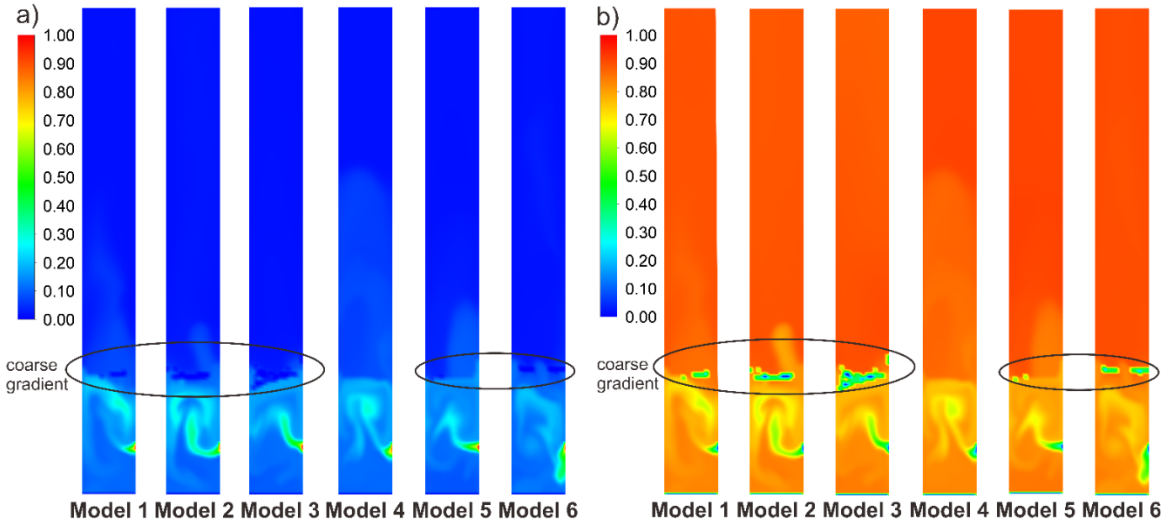


**Fig. 8. a) Biomass mass fraction; b) Char & metaplastic mass fraction.**

The char density affected the biomixture density, whereby a higher char density enhanced the biomixture density, indicated by the sharper gradient between the dense zone and the freeboard in Models 1 to 3 (Fig. 9a). Without implementation of the particle size reduction, the biomixture particles tended to accumulate in the dense zone, which promoted segregation. Similar to Models 1–3, the biomixture density of Models 4–6 increased with char density, with a more homogeneous density distribution correlated to the particle size shrinkage (Fig. 9b).

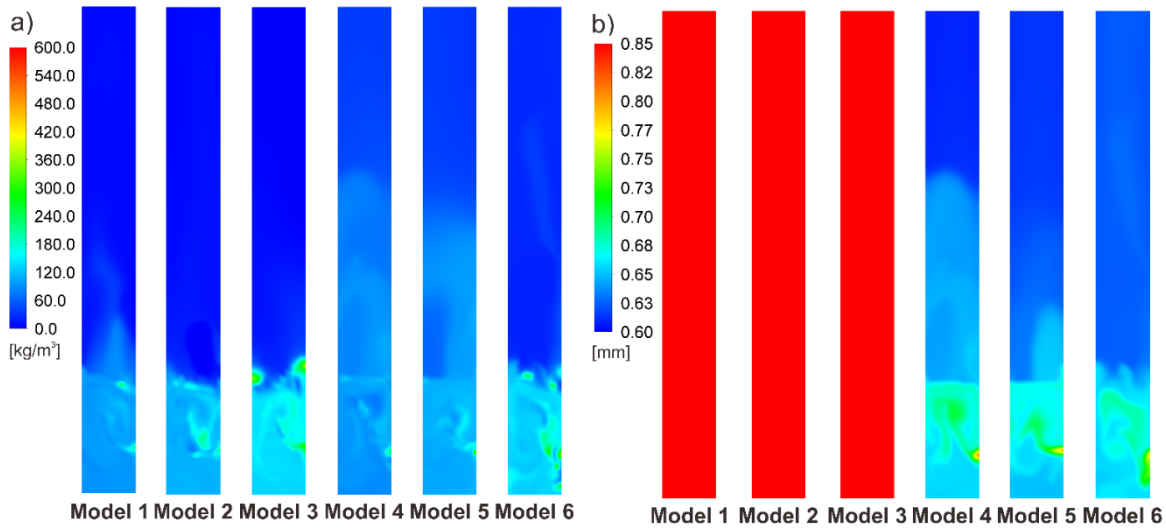


**Fig. 9. a) Biomixture particle density; b) Biomixture particle diameter.**

The evolution of biomass particles is depicted in Table 1. The average particle size and density increased with an increase in char density (Models 1–6); thus, the particle volume and density reduction were diminished by the increase in char density. Models 1–3 assumed that the particle size was constant; thus, no particle volume reduction occurred in these models. By contrast, in Models 4–6, the particle volume was reduced as the char density increased, namely, 54.5%, 54.3%, and 50.7% for 350, 600, and 2333 kg/m$^3$ of char density, respectively.

Davidsson and Pettersson [38] reported that birchwood pyrolysis resulted in 45%–70% particle volume reduction. In an experimental study conducted by Caposciutti et al. [39], particle volume reduction during the pyrolysis of beechwood particles was approximately 60%–66%. Kumar et al. [40] investigated particle shrinkage of casuarina wood during devolatilization in a fluidized bed reactor and reported that the volume of particles was reduced by approximately 35%–58%. Schröder [41] reported that the pyrolysis of large beechwood reduced the density, mass, and volume as the temperature increased. At approximately 500 °C, they were reduced to approximately 65%, 30%, and 45% from those of the initial biomass particle, respectively. In short, particle volume reduction ranges from 35% to 70%, and specifically for fluidized bed pyrolysis is about 35%–58%.

Correlating with the simulation results, Models 4–6 represented a proper particle shrinkage, where the particle volume reduction ranged from 35% to 58% according the literature for fluidized bed pyrolysis case.

**Table 1. Biomass particle evolution.**

| Case | Model 1 | Model 2 | Model 3 | Model 4 | Model 5 | Model 6 |
|---|---|---|---|---|---|---|
| Average final diameter (mm) | 0.85 | 0.85 | 0.85 | 0.654 | 0.654 | 0.672 |
| Average final density (kg/m$^3$) | 121.5 | 141.8 | 173.6 | 115.3 | 122.3 | 155.0 |
| Volume reduction (%) | 0.0 | 0.0 | 0.0 | 54.5 | 54.3 | 50.7 |
| Density reduction (%) | 79.8 | 76.4 | 71.1 | 80.8 | 79.6 | 74.2 |

Fig. 10 presents the pyrolysis product yields with their compositions and the corresponding particle shrinkage models. In general, the particle shrinkage models exhibited nonsignificant differences in the yields and compositions, by implementing the particle size shrinkage (Model 4–6) resulted in a little reduction in the solid residue yields (<1.0%) with a slightly higher carbon fraction in the same char density.

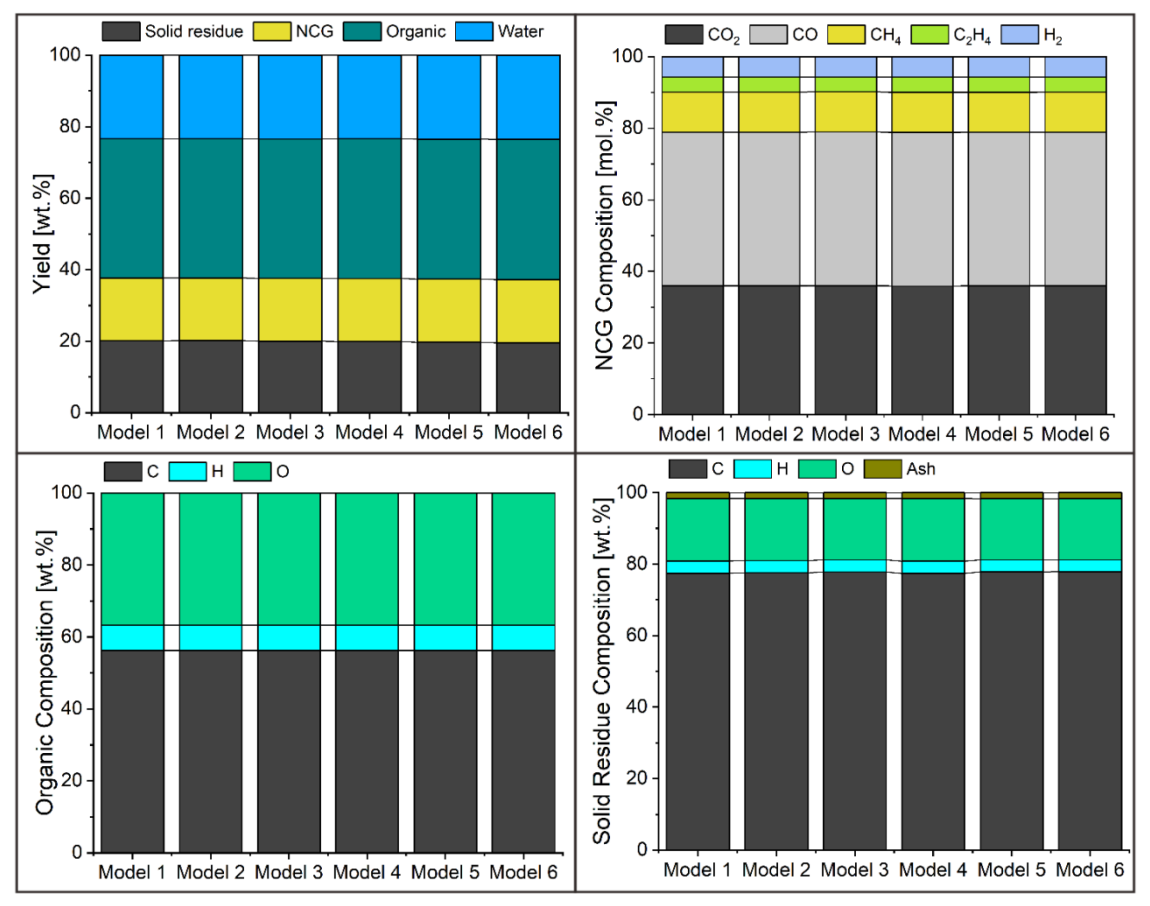


**Fig. 10. Comparison of pyrolysis yields and compositions of particle shrinkage models.**

## CONCLUSION AND SUGGESTION

The improvement of multistep comprehensive reaction with particle shrinkage models has been proposed for fast pyrolysis in a fluidized bed reactor. Various biomass particle sizes were also investigated to elucidate the particle behavior and biomass conversion characteristic in a fluidized bed reactor. The improved model successfully reduced the number of reaction steps to 24 and, overall, more accurately predicted solid residue, NCG, organic, and water outputs, with relative errors of 11.8%, −15.2%, 12.6%, and −8.0%, respectively. The organic product comprised carboxylic acids, ketones & aldehydes, furans, and phenolics, most of which were accurately predicted using the improved model. The organic elemental composition was satisfactorily estimated in the improved model, with C, H, and O compositions of 56.3%, 6.9%, and 36.8%, respectively. Implementing particle size shrinkage influenced the hydrodynamics behavior of biomass particle flow in the reactor, where both biomass and char & metaplastic mass fractions were distributed

more homogeneously in the reactor, especially observed in Model 4. Models 4–6 represented a proper particle size shrinkage; their volume reductions were 54.5%, 54.3%, and 50.7%, respectively. In addition, the particle shrinkage model did not significantly affect the pyrolysis yields and compositions.

**REFERENCES**

Jalalifar S, Abbassi R, Garaniya V, Salehi F, Papari S, Hawboldt K, et al. CFD Analysis of Fast Pyrolysis Process in a Pilot-Scale Auger Reactor. Fuel 2020;273:117782. https://doi.org/10.1016/j.fuel.2020.117782.

Guizani C, Valin S, Billaud J, Peyrot M, Salvador S. Biomass Fast Pyrolysis in a Drop Tube Reactor for Bio Oil Production: Experiments and Modeling. Fuel 2017;207:71–84. https://doi.org/10.1016/j.fuel.2017.06.068.

Clissold J, Jalalifar S, Salehi F, Abbassi R, Ghodrat M. Fluidisation Characteristics and Inter-Phase Heat Transfer on Product Yields in Bubbling Fluidised Bed Reactor. Fuel 2020;273:117791. https://doi.org/10.1016/j.fuel.2020.117791.

Thoharudin, Chen Y-S, Hsiau S-S. Numerical studies on fast pyrolysis of palm kernel shell in a fluidized bed reactor. IOP Conf. Ser. Mater. Sci. Eng., 2020. https://doi.org/10.1088/1757-899X/874/1/012033.

Jalalifar S, Abbassi R, Garaniya V, Hawboldt K, Ghiji M. Parametric Analysis of Pyrolysis Process on The Product Yields in a Bubbling Fluidized Bed Reactor. Fuel 2018;234:616–25. https://doi.org/10.1016/j.fuel.2018.07.070.

Miller RS, Bellan J. A generalized biomass pyrolysis model based on superimposed cellulose, hemicellulose and liqnin Kinetics. Combust Sci Technol 1997;126:97–137. https://doi.org/10.1080/00102209708935670.

Ranzi E, Cuoci A, Faravelli T, Frassoldati A, Migliavacca G, Pierucci S, et al. Chemical kinetics of biomass pyrolysis. Energy Fuels 2008;22:4292–300. https://doi.org/10.1021/ef800551t.

Anca-Couce A, Sommersacher P, Scharler R. Online experiments and modelling with a detailed reaction scheme of single particle biomass pyrolysis. J Anal Appl Pyrolysis 2017;127:411–25. https://doi.org/10.1016/j.jaap.2017.07.008.

Gentile G, Debiagi PEA, Cuoci A, Frassoldati A, Ranzi E, Faravelli T. A computational framework for the pyrolysis of anisotropic biomass particles. Chem Eng J 2017;321:458–73. https://doi.org/10.1016/j.cej.2017.03.113.

Debiagi P, Gentile G, Cuoci A, Frassoldati A, Ranzi E, Faravelli T. A predictive model of biochar formation and characterization. J Anal Appl Pyrolysis 2018;134:326–35. https://doi.org/10.1016/j.jaap.2018.06.022.

Mellin P, Kantarelis E, Yang W. Computational fluid dynamics modeling of biomass fast pyrolysis in a fluidized bed reactor, using a comprehensive chemistry scheme. Fuel 2014;117:704–15. https://doi.org/10.1016/j.fuel.2013.09.009.

Ranganathan P, Gu S. Computational Fluid Dynamics Modelling of Biomass Fast Pyrolysis in Fluidised Bed Reactors, Focusing Different Kinetic Schemes. Bioresour Technol 2016;213:333–41. https://doi.org/10.1016/j.biortech.2016.02.042.

Lu L, Gao X, Gel A, Wiggins GM, Crowley M, Pecha B, et al. Investigating biomass composition and size effects on fast pyrolysis using global sensitivity analysis and CFD simulations. Chem Eng J 2020;421:127789.

https://doi.org/10.1016/j.cej.2020.127789.
Ravenni G, Sárossy Z, Ahrenfeldt J, Henriksen UB. Activity of Chars and Activated Carbons for Removal and Decomposition of Tar Model Compounds – A Review. Renew Sustain Energy Rev 2018;94:1044–56. https://doi.org/10.1016/j.rser.2018.07.001.
Zhong H, Zhang J, Zhu Y, Liang S. Multi-fluid Modeling Biomass Fast Pryolysis with Particle Shrinkage Model for Complex Reaction Kinetics. Chem Eng Process Process Intensif 2018;128:36–45. https://doi.org/10.1016/j.cep.2018.03.030.
Zhong H, Xiong Q, Zhu Y, Liang S, Zhang J, Niu B, et al. CFD Modeling of the Effects of Particle Shrinkage and Intra-Particle Heat Conduction on Biomass Fast Pyrolysis. Renew Energy 2019;141:236–45. https://doi.org/10.1016/j.renene.2019.04.006.
Zhong H, Xiong Q, Yin L, Zhang J, Zhu Y, Liang S, et al. CFD-Based Reduced-Order Modeling of Fluidized-Bed Biomass Fast Pyrolysis using Artificial Neural Network. Renew Energy 2020;152:613–26. https://doi.org/10.1016/j.renene.2020.01.057.
Gómez-Barea A, Leckner B. Modeling of Biomass Gasification in Fluidized Bed. Prog Energy Combust Sci 2010;36:444–509. https://doi.org/10.1016/j.pecs.2009.12.002.
Yang S, Wang S, Wang H. Particle-Scale Evaluation of the Pyrolysis Process of Biomass Material in a Reactive Gas-Solid Spouted Reactor. Chem Eng J 2020;421:127787.
Liu B, Papadikis K, Gu S, Fidalgo B, Longhurst P, Li Z, et al. CFD Modelling of Particle Shrinkage in a Fluidized Bed for Biomass Fast Pyrolysis with Quadrature Method of Moment. Fuel Process Technol 2017;164:51–68.
Gidaspow D. Multiphase flow and fluidization. London: Academic Press; 1994. https://doi.org/10.1016/C2009-0-21244-X.
Gunn DJ. Transfer of heat or mass to particles in fixed and fluidised beds. Int J Heat Mass Transf 1978;21:467–76. https://doi.org/10.1016/0017-9310(78)90080-7.
Tomiyama A. Struggle with computational bubble dynamics. Multiph Sci Technol 1998;10:369–405. https://doi.org/10.1615/MultScienTechn.v10.i4.40.
Eri Q, Peng J, Zhao X. CFD simulation of biomass steam gasification in a fluidized bed based on a multi-composition multi-step kinetic model. Appl Therm Eng 2018;129:1358–68. https://doi.org/10.1016/j.applthermaleng.2017.10.122.
Ansys Fuent. Theory Guide. Canonsburg: Ansys Inc.; 2020.
Qian Y, Yu Y, Xu G, Liu X. CFD Modeling of Coal Pyrolysis in Externally Heated Fixed-Bed Reactor. Fuel 2018;233:685–94.
Kantarelis E, Yang W, Blasiak W. Production of liquid feedstock from biomass via steam pyrolysis in a fluidized bed reactor. Energy Fuels 2013;27:4748–59. https://doi.org/10.1021/ef400580x.
Thoharudin, Hsiau S-S, Chen Y-S, Yang S. Numerical simulation of fluidized bed pyrolysis under a simplified comprehensive multistep kinetic

mechanism: Effects of particle size and fluidization velocity. Energy Convers Manag 2022;254:115259. https://doi.org/10.1016/j.enconman.2022.115259.

Thoharudin, Hsiau S-S, Chen Y-S, Yang S. Numerical modeling of biomass fast pyrolysis by using an improved comprehensive reaction scheme for energy analysis. Renew Energy 2022;181:355–64. https://doi.org/10.1016/j.renene.2021.09.038.

Thoharudin, Hsiau S-S, Chen Y-S, Yang S. Design optimization of fluidized bed pyrolysis for energy and exergy analysis using a simplified comprehensive multistep kinetic model. Energy 2023;276:127615. https://doi.org/10.1016/j.energy.2023.127615.

Rößger P, Richter A. Numerical Modeling of a Batch Fluidized-Bed Gasifier: Interaction of Chemical Reaction, Particle Morphology Development and Hydrodynamics. Powder Technol 2021;384:148–59. https://doi.org/10.1016/j.powtec.2021.01.072.

Corbetta M, Frassoldati A, Bennadji H, Smith K, Serapiglia MJ, Gauthier G, et al. Pyrolysis of Centimeter-Scale Woody Biomass Particles: Kinetic Modeling and Experimental Validation. Energy Fuels 2014;28:3884–98. https://doi.org/10.1021/ef500525v.

Westerhof RJM, Kuipers NJM, Kersten SRA, van Swaaij WPM. Controlling the Water Content of Biomass Fast Pyrolysis Oil. Ind Eng Chem Res 2007;46:9238–47. https://doi.org/10.1021/ie070684k.

Chen T, Ku X, Li T, Karlsson BSA, Sjöblom J, Ström H. High-temperature pyrolysis modeling of a thermally thick biomass particle based on an MD-derived tar cracking model. Chem Eng J 2021;417:127923. https://doi.org/10.1016/j.cej.2020.127923.

Michailof C, Sfetsas T, Stefanidis S, Kalogiannis K, Theodoridis G, Lappas A. Quantitative and Qualitative Analysis of Hemicellulose, Cellulose and Lignin Bio-oils by Comprehensive Two-Dimensional Gas Chromatography with Time-of-Flight Mass Spectrometry. J Chromatogr A 2014;1369:147–60. https://doi.org/10.1016/j.chroma.2014.10.020.

Zhao C, Jiang E, Chen A. Volatile production from pyrolysis of cellulose, hemicellulose and lignin. J Energy Inst 2017;90:902–13. https://doi.org/10.1016/j.joei.2016.08.004.

Davidsson K., Pettersson JB. Birch Wood Particle Shrinkage during Rapid Pyrolysis. Fuel 2002;81:263–70. https://doi.org/10.1016/S0016-2361(01)00169-7.

Caposciutti G, Almuina-Villar H, Dieguez-Alonso A, Gruber T, Kelz J, Desideri U, et al. Experimental Investigation on Biomass Shrinking and Swelling Behaviour: Particles Pyrolysis and Wood Logs Combustion. Biomass and Bioenergy 2019;123:1–13. https://doi.org/10.1016/j.biombioe.2019.01.044.

Kumar RR, Kolar AK, Leckner B. Shrinkage Characteristics of Casuarina Wood during Devolatilization in a Fluidized Bed Combustor. Biomass and Bioenergy 2006;30:153–65. https://doi.org/10.1016/j.biombioe.2005.11.005.

Schröder E. Experiments on the Pyrolysis of Large Beechwood Particles in Fixed

Beds. J Anal Appl Pyrolysis 2004;71:669–94.
https://doi.org/10.1016/j.jaap.2003.09.004.
Wang C, Xia S, Yang X, Zheng A, Zhao Z, Li H. Oriented Valorization of Cellulose and Xylan into Anhydrosugars by using Low-Temperature Pyrolysis. Fuel 2021;291:120156.
https://doi.org/10.1016/j.fuel.2021.120156.